Rapid Electric Vehicle Charging Based on Silicon Carbide Enabled Medium Voltage DC Tranmission Systems.

DEB, Arkadeep <http://orcid.org/0000-0002-2776-3134>, GONZALEZ, Jose Ortiz <http://orcid.org/0000-0002-1461-3735>, WU, Ruizhu, ISSA, Walid <http://orcid.org/0000-0001-9450-5197>, JAHDI, Saeed <http://orcid.org/0000-0002-6471-0429> and ALATISE, Olayiwola <http://orcid.org/0000-0003-0993-2624>

Citation:

DEB, Arkadeep, GONZALEZ, Jose Ortiz, WU, Ruizhu, ISSA, Walid, JAHDI, Saeed and ALATISE, Olayiwola (2025). Rapid Electric Vehicle Charging Based on Silicon Carbide Enabled Medium Voltage DC Tranmission Systems. IET Generation, Transmission & Distribution, 19 (1): e70092. [Article]

IET Generation, Transmission & Distribution

WILEY

The Institution of Engineering and Technology

ORIGINAL RESEARCH OPEN ACCESS

Rapid Electric Vehicle Charging Based on Silicon Carbide Enabled Medium Voltage DC Tranmission Systems

Arkadeep Deb[1] | Jose Ortiz Gonzalez[1] | Ruizhu Wu[2] | Walid Issa[3] | Saeed Jahdi[4] | Olayiwola Alatise[1]

[1]School of Engineering, University of Warwick, Coventry, UK | [2]Chongqing Seres Phoenix Intelligent Innovation Technology Co., Ltd, Chongqing, China | [3]School of Engineering, Sheffield Hallam University, Sheffield, UK | [4]Faculty of Engineering, University of Bristol, Bristol, UK

Correspondence: Olayiwola Alatise (O.Alatise@warwick.ac.uk)

Received: 31 October 2024 | **Revised:** 2 May 2025 | **Accepted:** 6 May 2025

Funding: This study was supported by Royal Society Industry Fellowship (Grant/Award Number: INF R1 201014).

ABSTRACT

Rapid electric vehicle (EV) chargers with power ratings above 100 kW will become more common in the future. Reinforcing UK distribution networks with additional power handling capacity can be costly and disruptive. This is due to the limited headroom in 11 kV distribution networks and the high population densities where 11 kV/400 V transformers are located. This paper proposes a medium voltage DC (MVDC) system that bypasses the 33 kV/11 and 11 kV/400 V AC transformers by transmitting 54 kV DC power directly to the EV charging stations. The 33 kV AC to 54 kV rectification in this system is proposed to be done by using a 29-level modular multilevel converter (MMC) implemented in 3.3 kV SiC MOSFETs. On the EV side, there will be a 54 kV to 800 V/400 V fully isolated DC/DC converter implemented with 3.3 kV SiC MOSFETs on the primary side and 1.2 kV SiC MOSFETs or Schottky diodes on the secondary side. This paper presents experimentally calibrated converter simulation results demonstrating improved performance in the MVDC system and shows this is only possible with SiC MOSFET technology, as the losses using silicon IGBTs make the system less efficient than the existing AC transmission system.

1 | Introduction

In the future, when there is significant penetration of electric vehicles (EVs), the 11 kV distribution network will increasingly come under the stress of increased electric vehicle (EV) charging demand [1–5]. As a result, transformers in the distribution network will increasingly be loaded towards their electrical/thermal ratings. Various studies have shown the impact of increased EV charging on distribution transformers [6–10]. Studies in [11] showed the adverse impact of increased EV charging on the reliability of a distribution transformer due to increased thermal loading, while in [12], the impact of total harmonic distortion from the EV chargers on distribution transformers was analysed. Similar conclusions were reached in [8], where the winding hot-spot temperature on power distribution transformers was shown to increase with EV loading, and an off-peak tariff was recommended to redistribute the loading of the transformer. Other challenges aggravated by increased EV charging are voltage stability in distribution networks [13, 14]. The combination of increased EV charging and increased distributed generation (from rooftop photovoltaic systems) in the low voltage distribution system makes voltage control challenging [15].

Most studies, however, focus on residential charging, where Type 1 chargers (typically around 7 kW AC) are used for overnight charging. However, as EV numbers increase, daytime charging using type II and type III fast and ultra-fast charging will become commonplace. Increasing demand from heavy-duty EVs with large battery capacities (for example, electric buses) will also be the reality. Hence, ultra-fast charging during peak hours will become inevitable. The proliferation of ultra-fast chargers for heavy goods vehicles (HGVs) and electric buses will mean the

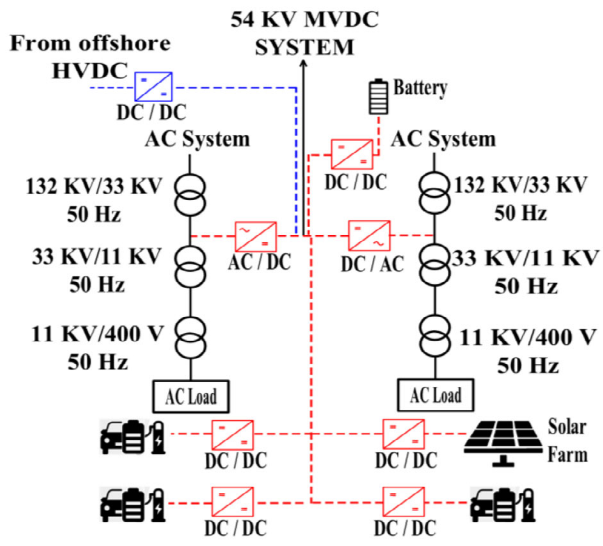

FIGURE 1 | Proposed MVDC Transmission in red.

demand for high-power EV chargers (100 kW and above) will increase [16–19]. This will require significant upgrades in the distribution network infrastructure, especially the 11 kV/400 V transformers. Integrating high-power chargers into the distribution network can be achieved in different ways, including (i) bundling low-voltage transformer capacities, (ii) using power supplies for light rail infrastructure where available and (iii) using medium-voltage DC (MVDC) technologies [20]. This paper proposes an MVDC transmission system that transmits power directly from the 33 kV AC system to the charging station. A conceptual diagram of this proposed system is illustrated in Figure 1 where the MVDC lines are shown in dashed lines, and the conventional AC lines are shown as solid lines. There are several advantages to this approach, namely

i. This approach avoids the need for upgrading several distribution transformers (33 kV/11 kV and 11 kV/400 V) since they are bypassed.
ii. By using MVDC transmission, different points in the low-voltage AC system can be interconnected, as would be the case when using a soft open point (SOP). The advantages of SOPs, which include increased improved network fault tolerance and more flexible active/reactive power flow, are well known [21].
iii. DC energy storage solutions like batteries and sources like photovoltaic generation can be more easily integrated into the DC transmission system.

The advantages of MVDC transmission are clear [22–25]. However, what remains to be assessed is the loss performance of the power converters compared to the conventional AC system and what role SiC power devices have to play. In [26], the use of 10 kV SiC MOSFETs in a medium-voltage (4.16 kV) connected fast charger was assessed. Given that 10 kV devices were used, a two-level active front-end rectifier was implemented for the EV charger. In [27], a modular multilevel DC-DC converter for EV chargers connected to MVDC systems was studied; however, there was no loss analysis performed. In [28], a medium voltage connected fast charging architecture was proposed for a charging station connected directly to a 4.16 kV grid. The converter was not an MMC-type topology, which didn't present a challenge given the relatively low AC side voltage.

In the system proposed in this study, rectification is performed at a higher voltage level (33 kV) and transmitted to the charging station using MVDC technology, completely bypassing the AC distribution system transformers. One of the main consequences of the proposed system is that different power electronic devices and converters are needed compared to the conventional system. The purpose of this study is to (i) assess the loss performance of the proposed system using the latest generation wide bandgap power semiconductor devices, namely high voltage (3.3 kV) SiC power MOSFETs and (ii) compare the losses with the conventional system.

This paper implements electrothermal simulations of EV charger power converters in the proposed MVDC system and compares them to the conventional AC system. Section 2 describes the proposed MVDC system in contrast with the existing AC system; Section 3 discusses the experimental measurements on the devices used in the simulations; Section 4 introduces the simulation methodology; Section 5 analyses the results and Section 6 concludes the paper.

2 | Proposed MVDC System

The current technology for EV charging solutions based on the 400 V system uses either on-board EV chargers (for type 1 and type 2 charging) or off-board chargers for type 3 DC fast charging [29, 30]. Both on-board and off-board EV chargers comprise a rectifier (for AC to DC conversion) and a DC/DC converter for interfacing with the EV battery. The rectifier can currently be implemented as a (i) Vienna rectifier, (ii) an active front-end rectifier [31] or (iii) a 12-pulse rectifier [32, 33]. The DC/DC converter is typically implemented using an isolated topology with a full bridge primary side converter, an isolating high-frequency transformer and either a full bridge diode rectifier (for unidirectional power flow) or another full bridge converter (for bidirectional power flow in vehicle-to-grid applications). In the conventional system, the EV charger is connected to the distribution network as shown in Figure 2. Here, there is a series of transformers between the main grid and the EV charging station. As has been shown in several studies, significant increases in EV charging will require reinforcement of the system, especially regarding the 11 kV/400 V distribution transformers [11, 34–38].

In the MVDC system proposed here, all the rectification is aggregated in the 33 kV bus. This means that this converter will have a significantly higher power rating since it will serve multiple rapid charging stations. Figure 3 shows a conceptual diagram of this proposed MVDC system with the high-power rectifier and the receiving end converters. 54 kV is chosen as the DC transmission voltage since this has been previously demonstrated in an MVDC system [22].

The high-voltage converters can be implemented as-

Two-Level H-bridge Converters with Series Connected Devices: In this topology, multiple devices will be connected

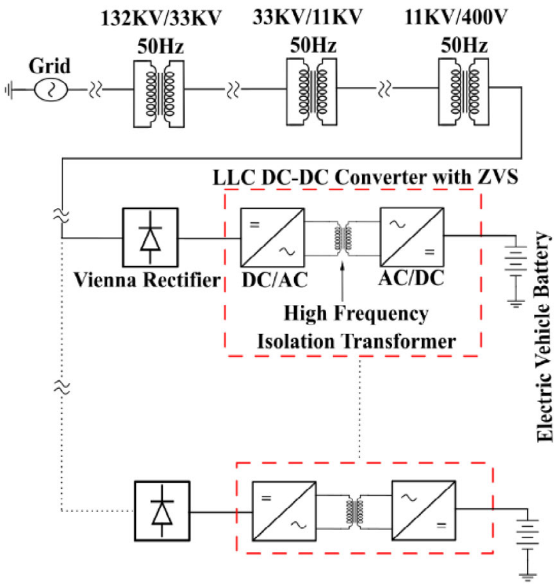

FIGURE 2 | EV charging system from 400 V AC mains.

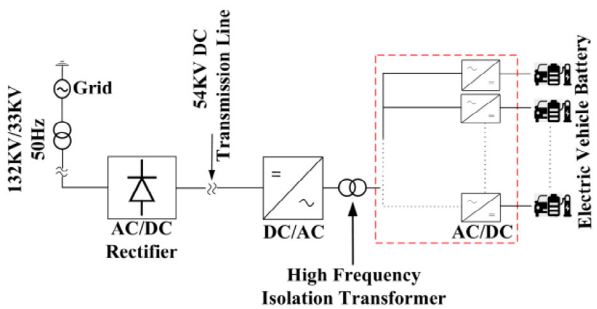

FIGURE 3 | EV Charging with MVDC.

in series for voltage sharing. Each of the six switching blocks of the H-bridge converter will be required to block the entire DC voltage (54 kV). Since the voltage blocking capability of commercially available power devices is limited to 3.3 kV (for SiC MOSFETs) and 6.5 kV (for silicon IGBTs), devices will have to be series connected to share the DC side voltage. This topology was initially commercialised by ABB in its first variant of voltage source converters for HVDC transmission systems. This topology comes with significant challenges, including static and dynamic voltage balancing, high electromagnetic stresses that come with fast switching, lack of fault tolerance due to no modularity and large filters for harmonic management [39].

Three level NPC Converters with Series Connected Devices [40]: In this topology, there are 12 switching units in the converter; hence, each unit is required to block half the DC link voltage. This means that the number of devices required for series connection in each switching unit is halved, thereby easing the difficulties mentioned earlier with two-level converters. The harmonic output of this converter is better than that of the two-level converter however, as there are more switching units, the control is slightly more complicated. This converter also lacks modularity and hence is also not fault tolerant.

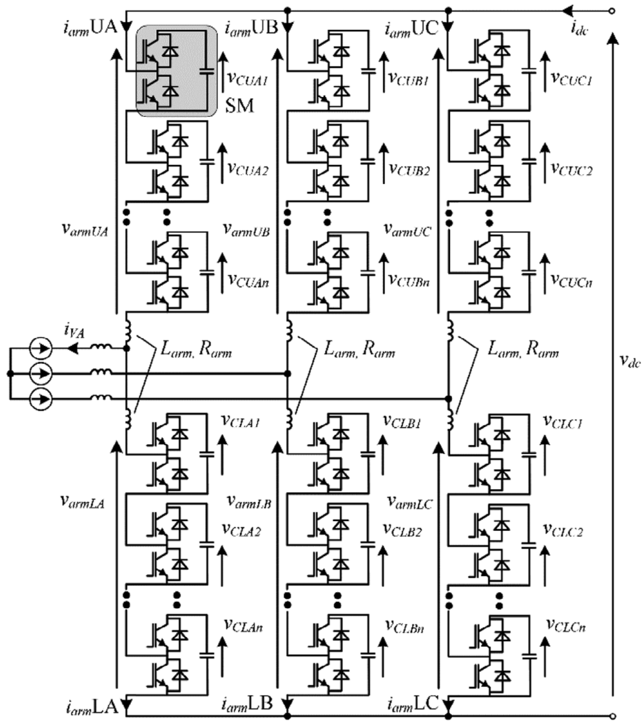

FIGURE 4 | MMC based three-phase rectifier for MVDC transmission to EV chargers.

Modular Multilevel Converter with Cascaded H-Bridges: In this topology, the DC link voltage is blocked by a series connection of half-bridge or full-bridge converters, each operating at a fraction of the total voltage depending on the number of levels. The primary advantage of this topology is the modularity since each submodule can be bypassed in case of failure in the devices, auxiliary electronics or passive components. This is advantageous from the perspective of fail-safe operation. Another main advantage of the MMC topology is the avoidance of series connection of power devices since each device only needs to block the submodule voltage. This submodule voltage will be the total voltage divided by the number of levels. The problems of static and dynamic voltage balancing are avoided. The switching losses of this converter are also significantly lower than those of 2 and 3L converters. Last, there is very little filtering requirement with this topology since a near-sinusoidal wave is produced. The THD performance is significantly better than those of 2 and 3L topologies. On the downside, the control system of this converter is significantly more complicated than series-connected 2L or NPC topologies.

Figure 4 shows the circuit diagram of an MMC-based MVDC rectifier that is proposed for use in this system. Since the DC side voltage is 54 kV and the converters at the EV charging station end will be required to step down from 54 kV to under 800 V or 400 V (for the EV battery), the converter topology applicable is not immediately clear, as this has not been demonstrated yet. This converter topology can come in 2 variants. One that uses a single-phase leg with series-connected capacitors on the MVDC link shown in Figure 5(a) and another that uses two phase legs with modular capacitors shown in Figure 5(B). In Figure 5(a), each arm is composed of unipolar submodules capable of generating

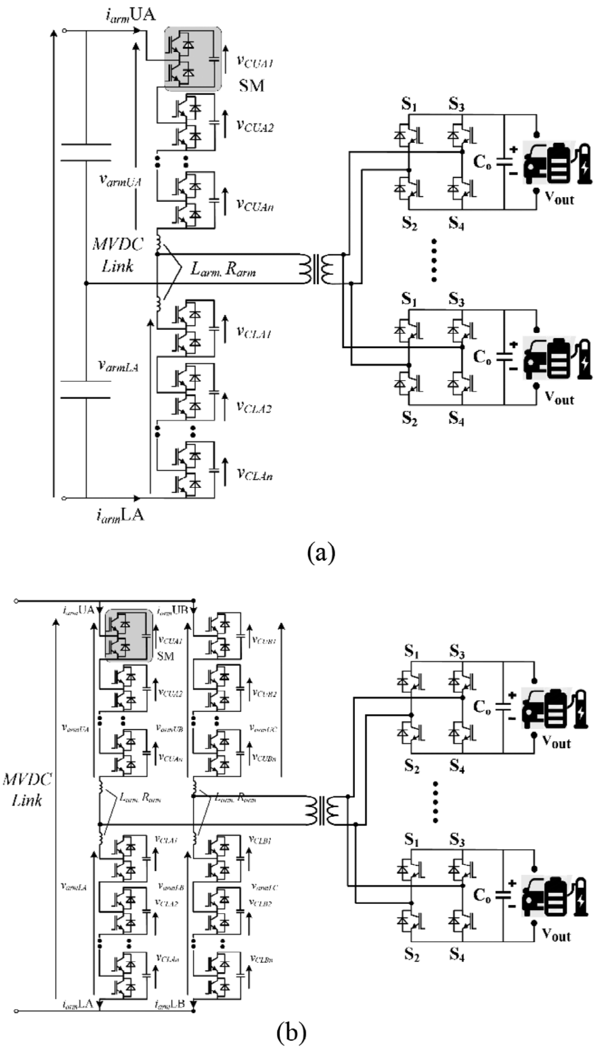

FIGURE 5 | Proposed DC/DC Converter based on MMC Topology **(A)** Half-bridge (one-leg) and **(B)** Full-bridge (two-leg).

voltages between 0 and the arm voltage (V_{ARM}), typically up to $V_{DC}/2$. By referencing the midpoint of the MVDC link as ground, the upper and lower arms are modulated symmetrically, resulting in a differential voltage across the transformer primary winding that spans from $-V_{DC}/2$ to $+V_{DC}/2$. This achieves a total voltage swing of V_{DC}, effectively creating a bipolar AC waveform across the transformer, despite each submodule being unipolar in nature. The differential connection helps eliminate the net DC offset, thus preventing magnetic core saturation. In contrast, the topology shown in Figure 5(B) utilises two independent legs (each with upper and lower arms), and the transformer is connected differentially between the midpoints of these legs. Through coordinated modulation of these four arms, the voltage at the transformer primary can swing from $-V_{DC}$ to $+V_{DC}$. This enables effective bipolar waveform synthesis. However, this extended voltage range also results in higher peak voltage stress across the transformer windings. Consequently, the transformer in the two-phase legs' configuration demands a more robust insulation design compared to the single-phase leg configuration, where the voltage stress is inherently limited to $\pm V_{DC}2$.

TABLE 1 | Devices used in EV Charger Simulations for both AC and MVDC transmission systems.

Device	I_{DS} @ 100°C	Datasheet
AC Transmission		
Vienna Rectifier Devices		
SiC MOSFET	650 V/27A	SCT3060AL
Silicon IGBTs	650 V/20A	RGTH40TS65D
SiC SBD	650 V/10A	C3D10065
DC/DC Converter Devices		
SiC MOSFET	1.2 kV/24A	C2M0080120D
Silicon IGBT	1.2 kV/20A	IHW20N120R5
SiC SBD	1.2 kV/16A	C4D10120A
MVDC Transmission		
MMC Rectifier Devices		
SiC MOSFET	3.3 kV/46A	G2R50MT33K
Silicon IGBT	6.5 kV/85A	QIC6508001
DC/DC Converter Devices		
SiC MOSFET	3.3 kV/46A	G2R50MT33K
SiC MOSFET	1.2 kV/395A	MSCSM120AM042 -CT6LIAG
Silicon IGBT	6.5 kV/85A	QIC6508001
Silicon IGBT	1.2 kV/400A	FZ400R12KE4

3 | Experimental Measurements of Switching Losses

In this section of the paper, the switching energies of the various devices have been measured. These devices include SiC MOSFETs, diodes and silicon IGBTs simulated in the Vienna rectifier, the LLC resonant DC/DC converter and the MMC. These measurements are used as inputs into the simulations described in the following sections to get more realistic and accurate assessments of the converter loss performance. Table 1 lists these devices alongside their respective datasheet references.

The clamped inductive switching test system and the circuit are shown in Figure 6. By charging up the inductor to a pre-defined current and switching the transistor, the turn-on and turn-off switching energies of the low side transistor and high side diode can be measured simultaneously. The switching energy is calculated from the measured waveforms using the equation below.

$$E_{SW-ON} = \int_{0}^{t_{on}} I_{DS} V_{DS} dt \quad (1)$$

Examples of the turn-on and turn-off measurements are shown in Figures 7(A) and (B), respectively. In these figures the drain current (I_{DS}), gate voltage (V_{GS}) and drain voltage (V_{DS}) transients are identified for the 1.2 kV SiC MOSFET switching 800 V and 30 A at a junction temperature of 25°C. These measurements were performed at 10 A, 20 A and 30 A with junction temperatures set

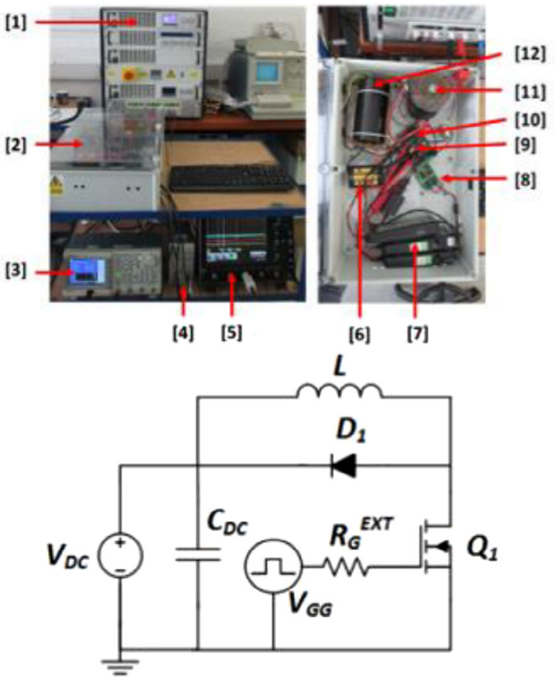

FIGURE 6 | Experimental test rig for measurement of switching transients. [1] DC Power Supply, [2] Test Enclosure, [3] Function Generator, [4] Current Probe Amplifier, [5] Oscilloscope, [6] DC Link Discharge Resistor, [7] Differential Probes [8] Gate Driver, [9] Current Probe (I_{SJ}), [10] DUT and Freewheeling Diode, [11] Inductor, [12] DC Link Capacitor.

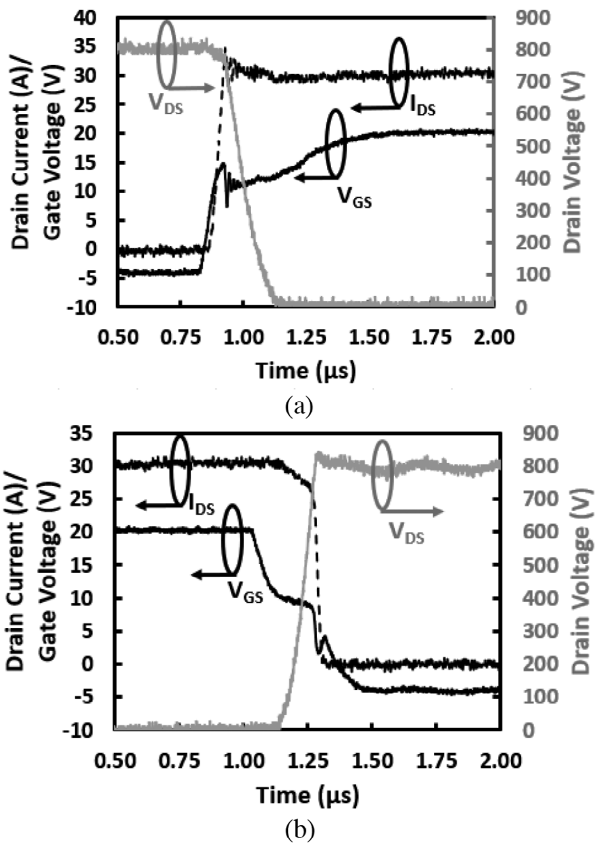

FIGURE 7 | Measured **(A)** Turn-On and **(B)** Turn-Off gate voltage, drain current and drain voltage transients.

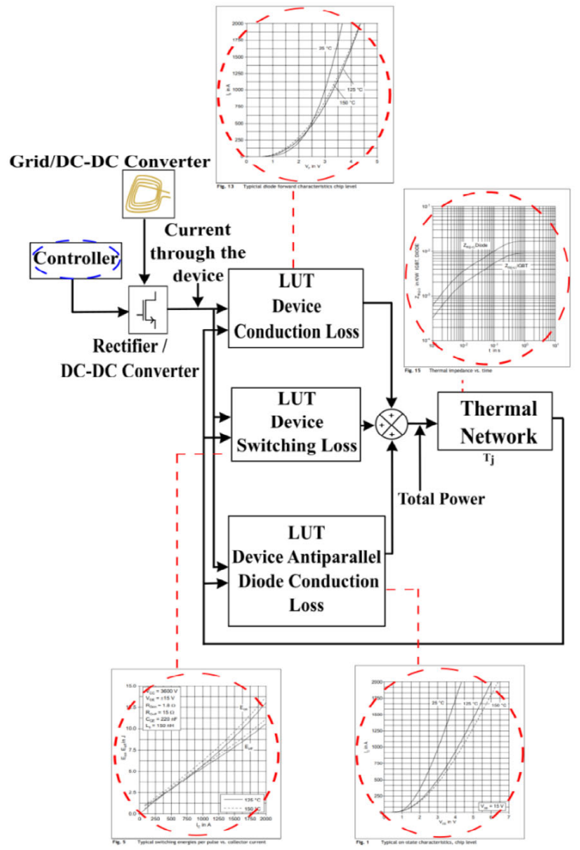

FIGURE 9 | Electrothermal Simulations for converter loss calculations.

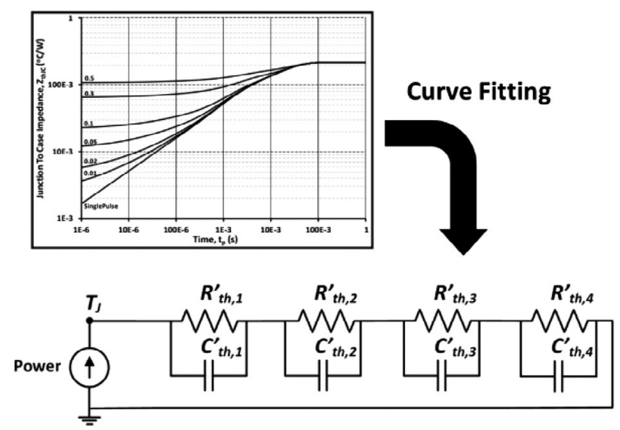

FIGURE 8 | Thermal network derivation from thermal impedance characteristics.

to 25°C, 75°C and 150°C. By measuring the switching energy at different temperatures and currents, a two-dimensional look-up table of measured losses was created and used in the simulations described in Figure 9.

The thermal impedances have been extracted from the datasheets and used in conjunction with the measured losses to give accurate junction temperatures for each device technology. This was done by using curve fitting on the transient thermal impedance characteristics to create a Foster thermal network as shown in Figure 8.

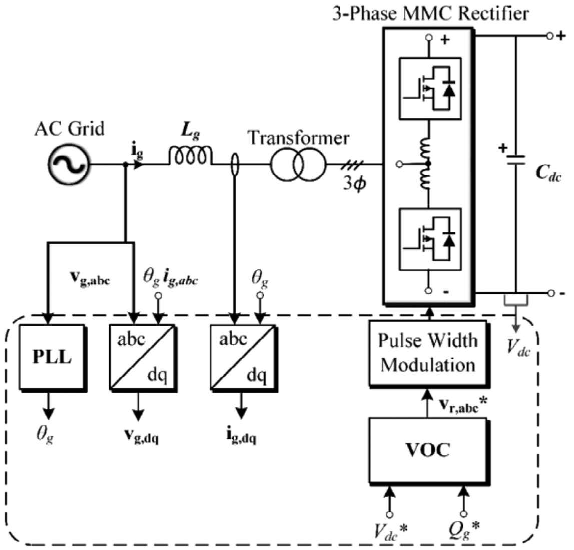

FIGURE 10 | Control block diagram of grid-side MMC rectifier.

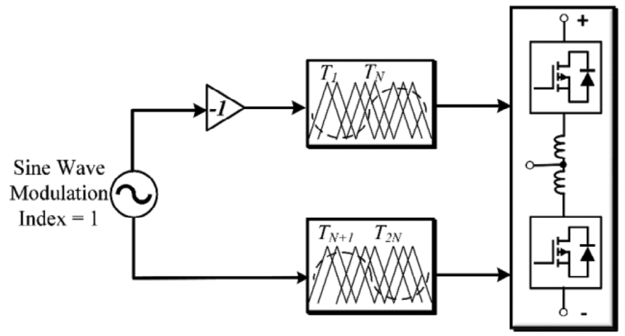

FIGURE 11 | Pulse width modulation for the MMC based rectifier and the primary side of the DC/DC converter.

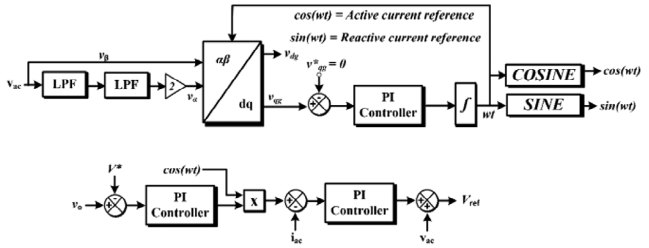

FIGURE 12 | Control algorithm for secondary side MMC based DC/DC converter.

The input to the Foster network is the instantaneous total loss, while the output is the device junction temperature. Figure 9 shows the electrothermal model of the converter and how a closed feedback loop between the losses and the junction temperature is achieved. As shown in Figure 9, the measured and datasheet values of the conduction and switching energies of the diodes and transistors are used to make the model fully electrothermal, thereby yielding accurate results. For each simulation time-step, the junction temperature computed in the previous step is used to select the device losses. This is acceptable since the junction temperature does not change instantaneously, and the simulation time step is well within the thermal time constant of the devices.

4 | Simulation Methodology

In this section of the paper, the electrothermal simulations in the previous section are performed on EV chargers in both the conventional low-voltage AC system and in the proposed MVDC system. To perform accurate loss calculations for the converters in the EV charging systems, it is first necessary to correctly simulate the control system of the converters. One of the widely used control schemes for grid-tied rectifiers is known as the voltage-oriented control (VOC) approach [41, 42]; hence, it is used for both the MVDC and the AC transmission system rectifiers.

4.1 | Simulation of MVDC-MMC Control System

The VOC approach was used for MVDC grid-tied-MMC based rectifiers, as shown in Figure 10. For the DC/DC converter, the primary side of the isolation transformer is subjected to open-loop control with a modulation index equal to 1. The modulated signal is fed into the phase-shifted carrier modulation scheme (PSC-PWM) block in MATLAB as shown in Figure 11 [43]. The assumption of a modulation index equal to 1 simplifies the analysis by ensuring that the converter operates at its maximum theoretical efficiency during the entire study. The control algorithm shown in Figure 12 is employed on the secondary side full-bridge rectifier shown in Figure 5(A). The v_{ac} (secondary side of the transformer AC voltage) is passed through two low-pass filters (LPF) and multiplied with a gain of 2 to generate a voltage signal same as v_{ac} with a phase shift of 90°. Therefore, v_{ac} is v_β and the output of LPF signal is v_α. Additionally, v_α and v_β are transformed to the DQ-reference frame. PLL is performed to find the angle which is in phase with the input voltage signal v_{ac}. The control is employed to ensure both zero reactive power and zero phase difference between voltage and current [44].

When simulating EV charging in the MVDC system, two power device technologies are assessed for the implementation. The highest-rated voltage SiC MOSFET commercially available is a 3.3 kV SiC MOSFET from GeneSiC with datasheet reference G2R50MT33K. Using this device will mean the MMC submodule voltage of 1928.57 V based on the device using 58.44% of its rated voltage capacity. This results in a 29-level MMC. If a 6.5 kV silicon IGBT is used, the number of levels of the MMC can be reduced to 17 since each submodule can be implemented with a voltage of 3375 V. The advantage of having a reduced number of levels is reduced complexity in the MMC control; however, the disadvantage can be higher THD.

Since there are no commercially available 6.5 kV SiC MOSFETs, this variant will have to be implemented in silicon IGBTs. For the simulation, a 6.5 kV IGBT from Powerex is used with datasheet reference QIC6508001. The fundamental frequency of the AC voltage produced by the primary side of the MMC converter is important because it will determine the size of the isolation transformer between the primary side and secondary side. The main advantage of solid-state transformers compared to conventional transformers is the smaller size of the isolation transformer since a higher fundamental frequency is used instead

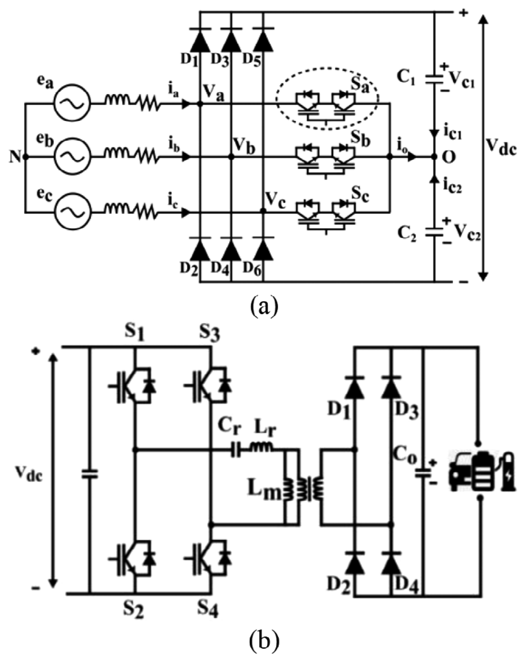

FIGURE 13 | Vienna rectifier and DC/DC converter used in AC based charging system.

of 50 Hz [45–47]. However, a higher fundamental frequency means a higher switching frequency, which translates into higher losses in the converter. Hence, there is a trade-off between power density and switching losses. In the simulations, a 1 kHz fundamental frequency is used with a 6 kHz switching frequency.

4.2 | Simulation of the Vienna Rectifier and LLC DC/DC Converter Control in AC Transmission System

The simulation employs the VOC for Vienna rectifier, and a voltage-controlled variable-frequency approach is adopted for the DC/DC Resonant LLC converter as in [48, 49]. The converter's switching frequency is carefully chosen to enable zero voltage switching (ZVS) during turn-on, thereby significantly reducing switching losses. Moreover, for gate signal generation, a modulated signal from the respective control algorithm is fed into the Sinusoidal PWM generator block in MATLAB.

Figure 13(A) shows the circuit diagram of the Vienna Rectifier, while Figure 13(B) shows that for the LLC DC/DC converter. In the simulations of the EV charger based on the 400 V AC system, referring to Figure 13(A), the bi-directional switches S_a, S_b and S_c are implemented in 650 V SiC MOSFETs and SiC SBDs. In the DC/DC converters in Figure 13(B), the switches S_1 and S_4 on the primary side of the converter are implemented in 1.2 kV SiC MOSFETs.

The switching transients are controlled by the PWM signals generated by the control system. Harmonic management of the rectifier is performed by the phase lock loop (PLL). Voltage and current control in the rectifier are implemented in the DQ reference frame as shown in Figure 14. An LLC converter is used for the DC/DC voltage control. The switching frequency of the converter is selected to ensure zero voltage switching (ZVS) at turn-on thereby reducing switching losses significantly. However, the turn-off losses of the transistors are still reflected in the converter's performance.

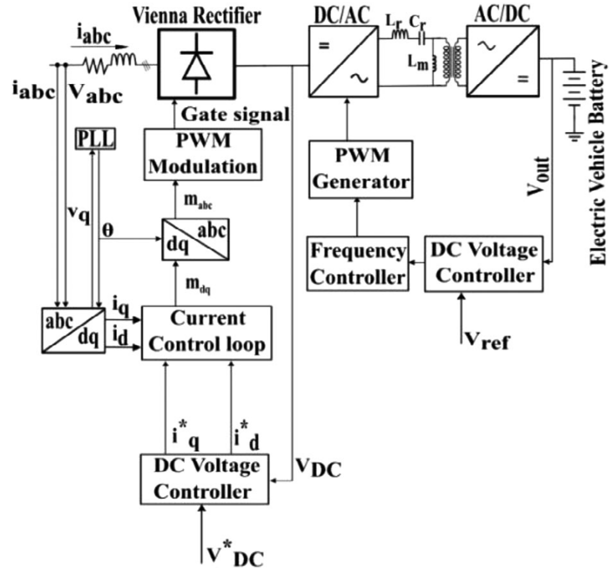

FIGURE 14 | Vienna rectifier control system implemented in Simulink.

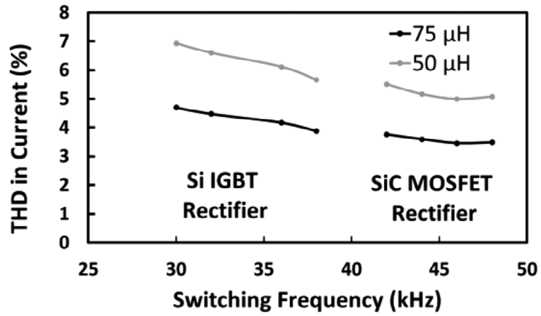

FIGURE 15 | Total harmonic distortion as a function switching frequency in Vienna rectifier.

The Vienna rectifier has been simulated with the Si IGBTs and SiC MOSFETs listed in Table 1. One of the main advantages of using SiC MOSFETs is the fact that reduced switching losses enable higher switching frequencies, which subsequently allow a reduction in the size of the passive components. Figure 15 shows the THD in the input current of the rectifier as a function of switching frequency for the Si IGBT-based and SiC MOSFET-based rectifiers. It can be seen in Figure 15 that using SiC MOSFETs allows smaller THD with smaller-sized line filtering inductances.

A key component in the design of soft-switched DC/DC converters is the component choice of the resonant tank that enables zero-voltage switching. The component of the resonant tank typically consists of a resonant inductor (L_r), a resonant capacitor (C_r), and sometimes an additional transformer magnetising inductance (L_m). The components of the resonant tank in this study have been selected using the standard LLC resonant design

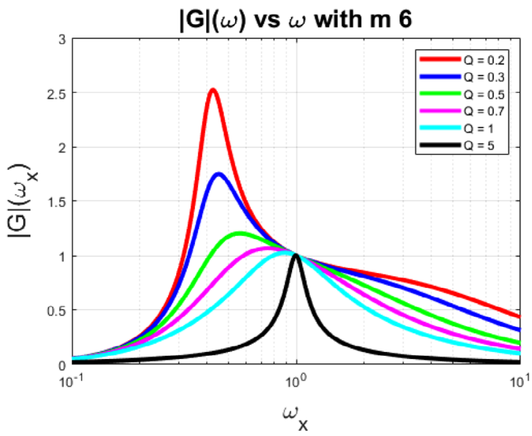

FIGURE 16 | LLC resonant tank gain (|G|(ω)) vs. frequency for varying Q, at fixed inductance ratio m = 6.

methodology outlined in [49]. The design procedure begins with defining critical operating parameters, such as nominal input and output voltages, rated power, switching frequency range, and desired ZVS load conditions. From these initial parameters, the transformer turns ratio ($\boldsymbol{n}$) and quality factor ($\boldsymbol{Q}$) are determined. The resonant tank is then characterised by two fundamental parameters: the resonant frequency ($\boldsymbol{f_r}$), defined as

$$f_r = \frac{1}{2\pi\sqrt{L_r C_r}}$$

and the ratio of magnetising inductance to resonance inductance (m), expressed as:

$$m = \frac{L_m}{L_r}$$

A smaller $\boldsymbol{m}$ ensures wider ZVS operation but increases circulating current and conduction losses, while a larger $\boldsymbol{m}$ improves efficiency at the cost of a narrower ZVS range.

Figure 16 shows the frequency response of the LLC resonant tank gain (|G|(ω)) for a range of quality factors ($\boldsymbol{Q}$), with a fixed inductance ratio $m = L_m \ / \ L_r = 6$. The gain characteristics highlight how the selection of the quality factor directly influences the resonant tank's peak gain and bandwidth. Lower $\boldsymbol{Q}$ values result in higher peak resonant gain but a narrower frequency range around resonance, which is suitable for applications requiring tight regulation around the resonant frequency. Conversely, higher $\boldsymbol{Q}$ values yield lower peak gain but broader frequency response, facilitating stable operation over a wider load range and improved robustness against frequency deviations. This gain analysis assists in selecting optimal resonant tank parameters to ensure efficient and reliable zero-voltage switching across the desired operating frequency range.

Figure 17 shows the resonant tank component values (inductor and capacitor) as a function of switching frequency. The higher switching frequencies enabled by SiC MOSFETs allow for more compact resonant tanks.

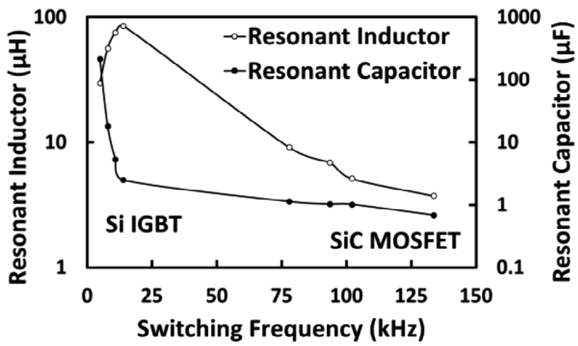

FIGURE 17 | DC/DC Converter LLC resonant tank components as a function of switching frequency.

4.3 | Junction Temperature Simulations

Junction temperatures have been estimated by using the datasheet-provided transient thermal impedances to generate thermal networks for each device. Figure 18 shows the loss calculation process for the EV charger where the turn-on, turn-off and conduction losses of the devices itemised in Table 1 are added into the total losses and used to compute the junction temperature. Figure 19 shows the simulated junction temperatures for the silicon IGBT/SiC SBD devices in the Vienna rectifier in comparison with the SiC MOSFET/SBD. Figure 20 shows the simulated junction temperatures of the devices in the DC/DC converter. It can be seen for both the rectifier and the DC/DC converter that the SiC MOSFETs have lower junction temperatures even though they are operated at higher switching frequencies. This is due to the lower switching losses in the SiC MOSFET.

5 | Results and Analysis

A 1 MW EV charging station is simulated. The peak current demand based on 1 MW charging power is used to determine the number of parallel devices in the simulations since the current conduction capacity of the discrete devices cannot be exceeded. On the primary side of the MVDC-based DC/DC converter shown in Figure 5(A), 3.3 kV/46A SiC MOSFETs are used due to the high voltages. On the secondary side of the DC/DC converter, due to the high currents needed by the EV battery, a 1.2 kV/395 A SiC MOSFET module is used (datasheet reference is in Table 1).

Figure 21 compares the simulation results of the power losses in the Vienna rectifier in the conventional 400 V AC charging system with those of the MMC converters in the 54 kV MVDC system. As a total charging power of 1 MW is assumed for the EV charging station, this breaks down to twenty-five EV chargers rated at 40 kW each. For the MVDC system, all the rectification is aggregated at the 33 kV bus on the sending end. The converters are simulated with losses from devices in Table 1 for technological comparison. Simulated losses for the MMC converters implemented in 3.3 kV SiC MOSFETs and 6.5 kV silicon IGBTs are also presented.

The results shown in Figure 21 using the SiC-based 29-level MMC converter yield the lowest losses. This is due to the improved

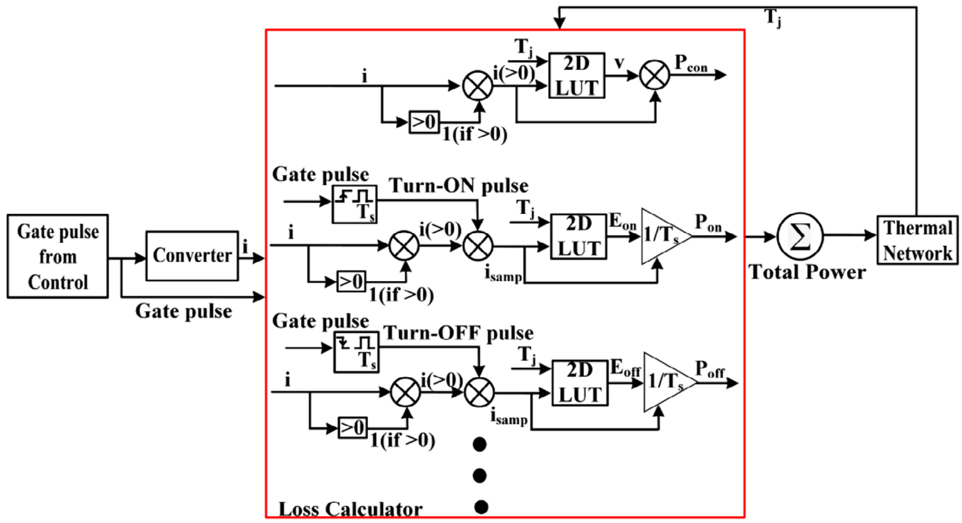

FIGURE 18 | Loss calculation process for Rectifier and DC/DC converter.

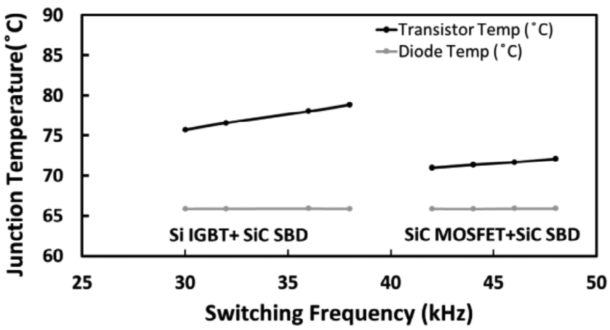

FIGURE 19 | Simulated junction temperature as a function of switching frequency for the devices in the Vienna rectifier.

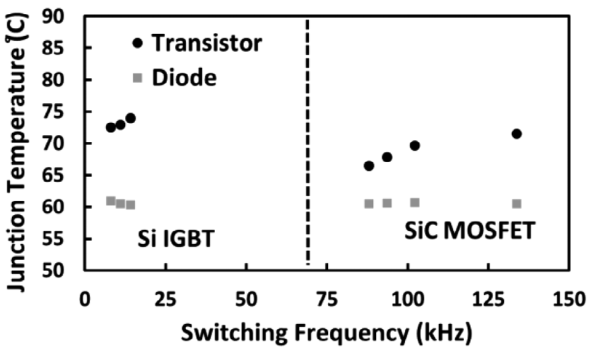

FIGURE 20 | Simulated junction temperature as a function of switching frequency for the devices in the DC/DC converter.

conduction and switching performance of SiC MOSFETs over IGBTs and the reduced switching frequencies inherent in MMC operation compared to Vienna rectifiers that operate at high switching frequencies. However, it should be noted that this converter will be significantly more expensive than the other solutions. The results in Figure 21 are important because it demonstrates that a single 1 MW MMC rectifier used in an MVDC system to convert all the energy required for the EV charging station is more efficient than twenty-five 40 kW Vienna rectifiers

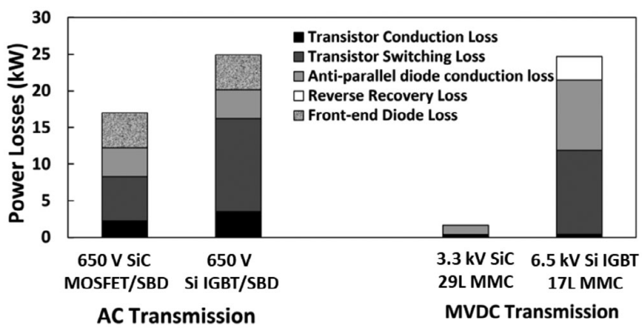

FIGURE 21 | Loss simulation for the rectifiers.

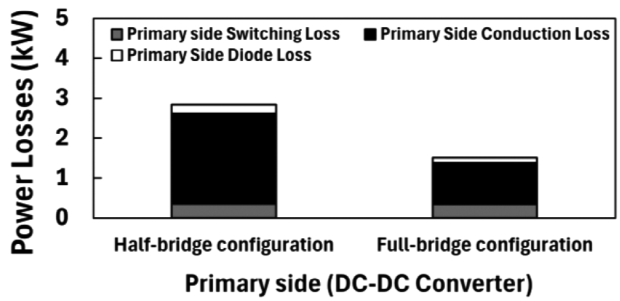

FIGURE 22 | Loss simulation MMC based DC/DC converter primary side.

in the traditional system. This analysis does not include the transmission losses related to the cables and the transformer losses in both transmission systems.

When considering which MMC variant to use for the MVDC-based EV charger, a choice must be made between the single-leg MMC topology shown in Figure 5(A) and the two-leg topology shown in Figure 5(B). The advantage of the single-phase leg topology is fewer power devices, while the advantage of the two-phase leg topology is increased modularity. Simulations have been performed on both variants to compare the losses. Figure 22 shows the loss comparison of both variants, demonstrating that

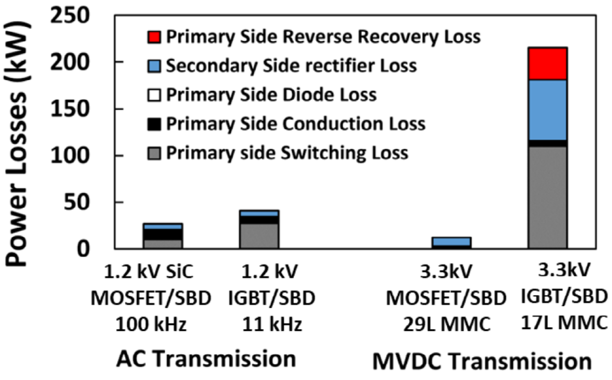

FIGURE 23 | Loss simulation for the DC/DC converters.

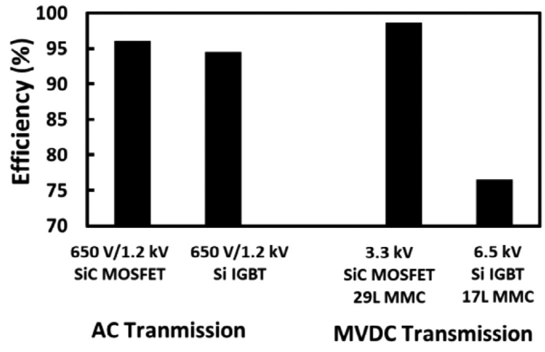

FIGURE 24 | Efficiency comparison.

the full-bridge configuration has less losses. The reduction in losses in the full-bridge topology is due to the smaller arm current resulting from the higher arm voltage (therefore the I^2R losses are lower). However, this loss reduction is not consequential because of the much higher secondary side losses.

Figure 23 shows the loss simulation results of the DC/DC conversion stage for the EV charger working from the AC transmission system and that working from the MVDC system. The losses include the conduction and switching losses of the primary side transistors as well as the total loss of the secondary side rectifiers. For the converter connected to the 400 V AC system, the SiC MOSFET-based converter is simulated with a 100 kHz switching frequency, while the Si IGBT-based converter is simulated with 11 kHz (due to limitations of the switching speed of silicon IGBTs).

This means that the SiC-based DC/DC converter will be significantly more compact since the isolating transformer will be significantly smaller.

The fundamental frequency used in the MMC-based DC/DC converter will determine the size of the isolation transformer; hence, in applications where space is limited, higher fundamental frequencies can be used, however, at the cost of higher switching losses (since the switching frequency will increase with the fundamental frequency). The MVDC converter on the primary side of the isolated DC/DC converter uses a fundamental frequency of 1 kHz to minimise the size of the isolating transformer. Again, the results show that the 29 level SiC based MMC converter demonstrates the best performance as it exhibits the lowest total losses. The 17 level MMC based on Si IGBTs exhibits significantly higher losses due to the switching losses of the Si IGBTs and the reverse recovery losses of the diode rectifiers in the secondary side. As there are no commercially available 6.5 kV SiC MOSFETs, the 17-level converter can only be implemented in Silicon IGBTs. Figure 24 compares the efficiencies of converters in the AC and MVDC transmission systems. Figure 24 shows that the MMC-MVDC charging system is only more efficient than the existing AC system if SiC MOSFET technology is used.

6 | Conclusions

This paper has proposed MVDC transmission technology as a preferable option for EV chargers over the conventional AC transmission system since it avoids the bottleneck of the lower voltage distribution transformers. Using electrothermal simulations of power converters in MATLAB Simulink coupled with experimentally measured device losses, it has been demonstrated that EV chargers based on MVDC-MMC transmission systems provide the best performance in terms of efficiency when implemented using SiC MOSFET technology. A 54 kV MVDC system for a 1 MW EV charging station was simulated using a 29-L MMC converter based on 3.3 kV SiC MOSFETs and compared to a 17-L MMC converter using 6.5 kV silicon IGBTs. This MMC-MVDC system is compared to EV chargers based on Vienna rectifiers and soft-switched DC/DC converters connected to the 400 V AC mains. The results show using MVDC transmission only yields better efficiency performance compared to the existing AC system when implemented in SiC MOSFET technology, which can yield significantly reduced switching losses at higher switching frequencies.

Author Contributions

Arkadeep Deb: investigation, methodology, validation and writing – original draft. **Jose-Ortiz Gonzalez:** formal analysis, methodology and project administration. **Ruizhu Wu:** investigation, methodology and software. **Walid Issa:** validation and visualisation. **Saeed Jahdi:** data curation, formal analysis and resources. **Olayiwola Alatise:** funding acquisition, investigation, supervision, writing – original draft, writing – review and editing.

Conflicts of Interest

The authors declare no conflicts of interest.

Data Availability Statement

Data sharing not applicable to this article as no datasets were generated or analysed during the current study.

References

1. L. P. Fernández, T. G. S. Roman, R. Cossent, C. M. Domingo, and P. Frías, "Assessment of the Impact of Plug-in Electric Vehicles on Distribution Networks," *IEEE Transactions on Power Systems* 26, no. 1 (2011): 206–213, https://doi.org/10.1109/TPWRS.2010.2049133.

2. G. Pisano, S. Ruggeri, G. G. Soma, D. Falabretti, S. Grillo, and F. Gulotta, "Impact of Electrical Vehicle Private Charging Stations on the Quality of the Low Voltage Network Supply," *IEEE Open Access Journal of Power and Energy* 10 (2023): 351–362, https://doi.org/10.1109/OAJPE.2023.3258254.

3. K. Clement-Nyns, E. Haesen, and J. Driesen, "The Impact of Charging Plug-In Hybrid Electric Vehicles on a Residential Distribution Grid," *IEEE Transactions on Power Systems* 25, no. 1 (2010): 371–380, https://doi.org/10.1109/TPWRS.2009.2036481.

4. P. V. Harisyam, S. Kasicheyanula, S. Mathapati, and K. Basu, "A Three-phase MVAC to Multi-port LVDC Converter With High Frequency Isolation for Fast DC Charging Station for EVs," in *Proceedings of the 2023 IEEE Energy Conversion Congress and Exposition (ECCE)*, October 29–November 2, 2023, (IEEE, 2023), 33–38, https://doi.org/10.1109/ECCE53617.2023.10362814.

5. I. Nutkani, H. Toole, N. Fernando, and L. P. C. Andrew, "Impact of EV Charging on Electrical Distribution Network and Mitigating Solutions – A Review," *IET Smart Grid* 7, no. 5 (2024): 485–502, https://doi.org/10.1049/stg2.12156.

6. A. G. Anastasiadis, G. P. Kondylis, A. Polyzakis, and G. Vokas, "Effects of Increased Electric Vehicles Into a Distribution Network," *Energy Procedia* 157 (2019): 586–593, https://doi.org/10.1016/j.egypro.2018.11.223.

7. L. Cheng, Y. Chang, Q. Wu, W. Lin, and C. Singh, "Evaluating Charging Service Reliability for Plug-In EVs from the Distribution Network Aspect," *IEEE Transactions on Sustainable Energy* 5, no. 4 (2014): 1287–1296, https://doi.org/10.1109/TSTE.2014.2348575.

8. R. Godina, E. M. G. Rodrigues, N. G. Paterakis, O. Erdinc, and J. P. S. Catalão, "Innovative Impact Assessment of Electric Vehicles Charging Loads on Distribution Transformers Using Real Data," *Energy Conversion and Management* 120 (2016): 206–216, https://doi.org/10.1016/j.enconman.2016.04.087.

9. Y. Chen, A. Oudalov, and J. S. Wang, "Integration of Electric Vehicle Charging System Into Distribution Network," in *Proccedings of the 8th International Conference on Power Electronics—ECCE Asia*, May 30 – June 3, 2011, (IEEE, 2011), 593–598, https://doi.org/10.1109/ICPE.2011.5944615.

10. G. A. Putrus, P. Suwanapingkarl, D. Johnston, E. C. Bentley, and M. Narayana, "Impact of Electric Vehicles on Power Distribution Networks," in *Proceedings of the 2009 IEEE Vehicle Power and Propulsion Conference*, September 7–10, 2009, (IEEE, 2009), 827–831, https://doi.org/10.1109/VPPC.2009.5289760.

11. M. J. Rutherford and V. Yousefzadeh, "The Impact of Electric Vehicle Battery Charging on Distribution Transformers," in *Proceedings of the 2011 Twenty-Sixth Annual IEEE Applied Power Electronics Conference and Exposition (APEC)*, March 6–11, 2011), (IEEE, 2011), 396–400, https://doi.org/10.1109/APEC.2011.5744627.

12. J. C. Gomez and M. M. Morcos, "Impact of EV Battery Chargers on the Power Quality of Distribution Systems," *IEEE Transactions on Power Delivery* 18, no. 3 (2003): 975–981, https://doi.org/10.1109/TPWRD.2003.813873.

13. K. Gholami, S. Karimi, A. Rastgou, A. Nazari, and V. Moghaddam, "Voltage Stability Improvement of Distribution Networks Using Reactive Power Capability of Electric Vehicle Charging Stations," *Computers and Electrical Engineering* 116 (2024): 109160, https://doi.org/10.1016/j.compeleceng.2024.109160.

14. J. Then, A. P. Agalgaonkar, and K. M. Muttaqi, "Hosting Capacity of an Australian Low-Voltage Distribution Network for Electric Vehicle Adoption," *IEEE Transactions on Industry Applications* 60, no. 2 (2024): 2601–2610, https://doi.org/10.1109/TIA.2023.3337068.

15. J. Then, A. P. Agalgaonkar, and K. M. Muttaqi, "Coordinated Charging of Spatially Distributed Electric Vehicles for Mitigating Voltage Rise and Voltage Unbalance in Modern Distribution Networks," *IEEE Transactions on Industry Applications* 59, no. 4 (2023): 5149–5157, https://doi.org/10.1109/TIA.2023.3273186.

16. W. Shoman, S. Yeh, F. Sprei, P. Plötz, and D. Speth, "Battery Electric Long-Haul Trucks in Europe: Public Charging, Energy, and Power Requirements," *Transportation Research Part D: Transport and Environment* 121 (2023): 103825, https://doi.org/10.1016/j.trd.2023.103825.

17. O. Alatise, A. Deb, E. Bashar, J. Ortiz Gonzalez, S. Jahdi, and W. Issa, "A Review of Power Electronic Devices for Heavy Goods Vehicles Electrification: Performance and Reliability," *Energies* 16, no. 11 (2023): 4380, https://doi.org/10.3390/en16114380.

18. C. de Saxe, D. Ainalis, J. Miles, et al., "Vehicle and Charging Requirements for an Electrified Road Freight System Demonstrator in the UK," *Transportation Research Procedia* 72 (2023): 4033–4040, https://doi.org/10.1016/j.trpro.2023.11.375.

19. A. Ahmad, Z. Qin, T. Wijekoon, and P. Bauer, "An Overview on Medium Voltage Grid Integration of Ultra-Fast Charging Stations: Current Status and Future Trends," *IEEE Open Journal of the Industrial Electronics Society* 3 (2022): 420–447, https://doi.org/10.1109/OJIES.2022.3179743.

20. M. Stieneker, B. J. Mortimer, A. Hinz, A. Müller-Hellmann, and R. W. D. Doncker, "MVDC Distribution Grids for Electric Vehicle Fast-Charging Infrastructure," in *2018 International Power Electronics Conference (IPEC-Niigata 2018 -ECCE Asia)*, May 20–24, 2018, (IEEE, 2018), 598–606, https://doi.org/10.23919/IPEC.2018.8507594.

21. X. Jiang, Y. Zhou, W. Ming, P. Yang, and J. Wu, "An Overview of Soft Open Points in Electricity Distribution Networks," *IEEE Transactions on Smart Grid* 13, no. 3 (2022): 1899–1910, https://doi.org/10.1109/TSG.2022.3148599.

22. G. Bathurst, G. Hwang, and L. Tejwani, "MVDC—The New Technology for Distribution Networks," in *Proceedings of the 11th IET International Conference on AC and DC Power Transmission*, February10–12, 2015, (IET, 2015), 1–5, https://doi.org/10.1049/cp.2015.0037.

23. J. K. Steinke, P. Maibach, G. Ortiz, F. Canales, and P. Steimer, "MVDC Applications and Technology," in *Proceedings of the PCIM Europe 2019; International Exhibition and Conference for Power Electronics, Intelligent Motion, Renewable Energy and Energy Management*, May 7–9, 2019, (VDE, 2019), 1–8.

24. E. C. Mathew and A. Das, "Integration of Renewable Energy Sources With MVDC Network," in *Proceedings of the 2020 IEEE International Conference on Power Electronics, Drives and Energy Systems (PEDES)*, December16–19, 2020, (IEEE, 2020), 1–6, https://doi.org/10.1109/PEDES49360.2020.9379756.

25. G. F. Reed, B. M. Grainger, A. R. Sparacino, E. J. Taylor, M. J. Korytowski, and Z.-H. Mao, "Medium Voltage DC Technology Developments, Applications, and Trends," 2012.

26. G. V. Bharath, S. K. Voruganti, V. T. Nguyen, V. U. Pawaskar, and G. Gohil, "Performance Evaluation of 10 kV SiC-based Extreme Fast Charger for Electric Vehicles With Direct MV AC Grid Interconnection," in *Proceedings of the 2020 IEEE Applied Power Electronics Conference and Exposition (APEC)*, March 15–19, 2020, (IEEE, 2020), 3547–3554, https://doi.org/10.1109/APEC39645.2020.9124089.

27. S. Sarkar and A. Das, "An Isolated Single Input-Multiple Output DC–DC Modular Multilevel Converter for Fast Electric Vehicle Charging," *IEEE Journal of Emerging and Selected Topics in Industrial Electronics* 4, no. 1 (2023): 178–187, https://doi.org/10.1109/JESTIE.2022.3221006.

28. A. Bahrami and M. Narimani, "A New Medium-Voltage Architecture for Ultra-Fast Electric Vehicle (EV) Charging Stations," in *Proceedings of the 2023 IEEE Applied Power Electronics Conference and Exposition (APEC)*, March 19–23, 2023, (IEEE, 2023), 3111–3118, https://doi.org/10.1109/APEC43580.2023.10131389.

29. H. Wouters and W. Martinez, "Bidirectional Onboard Chargers for Electric Vehicles: State-of-the-Art and Future Trends," *IEEE Transactions on Power Electronics* 39, no. 1 (2024): 693–716, https://doi.org/10.1109/TPEL.2023.3319996.

30. A. Khaligh and M. D. Antonio, "Global Trends in High-Power on-Board Chargers for Electric Vehicles," *IEEE Transactions on Vehicular Technology* 68, no. 4 (2019): 3306–3324, https://doi.org/10.1109/TVT.2019.2897050.

31. A. Zhaksylyk, H. Rasool, E. Abramushkina, et al., "Review of Active Front-End Rectifiers in EV DC Charging Applications," *Batteries* 9, no. 3 (2023): 150, https://doi.org/10.3390/batteries9030150.

32. M. Taha, A. Almaktoof, and M. T. E. Khan, "12 Pulse High Power Active Rectifier for Electric Vehicle Charging," *Transportation Research Procedia* 70 (2023): 299–306, https://doi.org/10.1016/j.trpro.2023.11.033.

33. D. Lan, Y. Wu, T. B. Soeiro, P. Granello, Z. Qin, and P. Bauer, "12-pulse Rectifier With DC-Side Buck Converter for Electric Vehicle Fast Charging," in *IECON 2022 – 48th Annual Conference of the IEEE Industrial Electronics Society*, October17–20, 2022, (IEEE, 2022), 1–6, https://doi.org/10.1109/IECON49645.2022.9968872.

34. M. Kazerooni and N. C. Kar, "Impact Analysis of EV Battery Charging on the Power System Distribution Transformers," in *Proceedings of the 2012 IEEE International Electric Vehicle Conference*, March 4–8, 2012, (IEEE, 2012), 1–6, https://doi.org/10.1109/IEVC.2012.6183254.

35. O. Alatise, A. Karlsson, A. Deb, R. Wu, and J. Ortiz-Gonzalez, "Expanding EV Charging Capacity in Distribution Networks: A Case Study for Charging EVs at Work," *IET Conference Proceedings*, 2021, 6, 2945–2949, 2021, https://doi.org/10.1049/icp.2021.1919.

36. Q. Gong, S. Midlam-Mohler, V. Marano, and G. Rizzoni, "Study of PEV Charging on Residential Distribution Transformer Life," *IEEE Transactions on Smart Grid* 3, no. 1 (2012): 404–412, https://doi.org/10.1109/TSG.2011.2163650.

37. A. D. Hilshey, P. D. H. Hines, and J. R. Dowds, "Estimating the Acceleration of Transformer Aging due to Electric Vehicle Charging," in *Proceedings of the 2011 IEEE Power and Energy Society General Meeting*, July 24–28, 2011, (IEEE, 2011), 1–9, https://doi.org/10.1109/PES.2011.6039848.

38. K. Qian, C. Zhou, and Y. Yuan, "Impacts of High Penetration Level of Fully Electric Vehicles Charging Loads on the Thermal Ageing of Power Transformers," *International Journal of Electrical Power & Energy Systems* 65 (2015): 102–112, https://doi.org/10.1016/j.ijepes.2014.09.040.

39. N. Flourentzou, V. G. Agelidis, and G. D. Demetriades, "VSC-Based HVDC Power Transmission Systems: An Overview," *IEEE Transactions on Power Electronics* 24, no. 3 (2009): 592–602, https://doi.org/10.1109/TPEL.2008.2008441.

40. A. Mortezaei, M. Abdul-Hak, and M. G. Simoes, "A Bidirectional NPC-based Level 3 EV Charging System With Added Active Filter Functionality in Smart Grid Applications," in *Proceedings of the 2018 IEEE Transportation Electrification Conference and Expo (ITEC)*, June 13–15, 2018, (IEEE, 2018), 201–206, https://doi.org/10.1109/ITEC.2018.8450196.

41. D. Sixing, D. Apparao, W. Bin, and Z. Navid, "Modular Multilevel Converter Based Medium-Voltage Motor Drives," *Modular Multilevel Converters: Analysis, Control, and Applications*. (IEEE, 2018): 229–270.

42. K. Matiyali, S. K. Goel, and H. Joshi, "Voltage Oriented Control of Grid-tied Solar PV System," in *Proceedings of the 2019 Women Institute of Technology Conference on Electrical and Computer Engineering (WITCON ECE)*, November22–23, 2019, (IEEE, 2019), 28–34, https://doi.org/10.1109/WITCONECE48374.2019.9092933.

43. D. Sixing, D. Apparao, W. Bin, and Z. Navid, "Fundamentals of Modular Multilevel Converter," *Modular Multilevel Converters: Analysis, Control, and Applications*. (IEEE, 2018): 37–78.

44. S. Gao and M. Barnes, "Phase-Locked Loop for AC Systems: Analyses and Comparisons," in *Proceedings of the 6th IET International Conference on Power Electronics, Machines and Drives (PEMD 2012)*, March 27–29, 2012, (IET, 2012), 1–6, https://doi.org/10.1049/cp.2012.0199.

45. X. She and A. Huang, "Solid State Transformer in the Future Smart Electrical System," in *Proceedings of the 2013 IEEE Power & Energy Society General Meeting*, July 21–25, 2013, (IEEE, 2013), 1–5, https://doi.org/10.1109/PESMG.2013.6672768.

46. M. Leibl, G. Ortiz, and J. W. Kolar, "Design and Experimental Analysis of a Medium-Frequency Transformer for Solid-State Transformer Applications," *IEEE Journal of Emerging and Selected Topics in Power Electronics* 5, no. 1 (2017): 110–123, https://doi.org/10.1109/JESTPE.2016.2623679.

47. M. A. Hannan, P. J. Ker, M. S. H. Lipu, et al., "State of the Art of Solid-State Transformers: Advanced Topologies, Implementation Issues, Recent Progress and Improvements," *IEEE Access* 8 (2020): 19113–19132, https://doi.org/10.1109/ACCESS.2020.2967345.

48. T. Taufik, M. McCarthy, S. Watkins, and M. Anwari, "Performance Study of Series Loaded Resonant Converter Using Super Barrier Rectifiers," in *Proceedings of the TENCON 2009 - 2009 IEEE Region 10 Conference*, January 23–26, 2009, (IEEE, 2009), 1–5, https://doi.org/10.1109/TENCON.2009.5395978.

49. S. Abdel-Rahman, "Application Note AN 2012-09 V1.0: Resonant LLC Converter: Operation and Design 250 W 33Vin 400Vout Design Example." [Online]. Available, https://www.infineon.com/dgdl/Application_Note_Resonant+LLC+Converter+Operation+and+Design_Infineon.pdf?fileId=db3a30433a047ba0013a4a60e3be64a1.